CHEMISTRY OF MATERIALS

ARTICLE

pubs.acs.org/cm

Layer-by-Layer Assembled Solid Polymer Electrolyte for Electrochromic Devices

Chien A. Nguyen,[†,∥] Avni A. Argun,[§] Paula T. Hammond,[*,§] Xuehong Lu,[†,‡] and Pooi See Lee[*,†,‡]

[†]Temasek Laboratories, Nanyang Technological University, 50 Nanyang Drive, Singapore 637552

[‡]School of Materials Science and Engineering, Nanyang Technological University, 50 Nanyang Avenue, Singapore 639798

[§]Department of Chemical Engineering, Massachusetts Institute of Technology, Cambridge, Massachusetts 02139, United States

Supporting Information

ABSTRACT: A new solid polymer electrolyte film fabricated by layer-by-layer (LbL) assembly is presented. The electrolyte film consists of four interbonding layers per deposition cycle, which combines electrostatic and hydrogen bonding in the same structure. Linear poly(ethylene imine) (LPEI) and poly(ethylene oxide) (PEO) are used to enhance the dissolution of lithium salt and the ionic transport through segmental motions of polymer chains. Characterization of film structure and growth shows good incorporation of electrostatic and hydrogen bonding, because of the versatile control of the ionization of poly(acrylic acid) (PAA), which serves as a bridging molecule. Ionic conductivity values, as described by the Vogel−Fulcher−Tammann equation, are found to be above 10^{-5} S/cm for the dried electrolyte at room temperature and moderate humidity (52%RH). Thermal analysis reveals two competing processes, namely, cross-linking of LPEI and PAA to form an amide compound and segregation of PEO crystalline phase, which results in a moderate reduction of conductivity in the electrolyte after heating. Demonstration of solid electrochromic devices using the LbL-assembled polymer electrolyte is presented in both transmission and reflection mode with a modulation of 30%−40% in the visible and near-infrared range. The successful fabrication of the LbL-assembled electrolytes enables the realization of completely flexible, polymeric, and solid electrochromic devices.

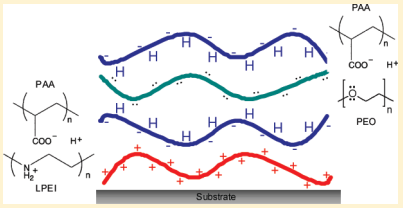

KEYWORDS: layer-by-layer assembly, solid polymer electrolyte, electrochromic device

INTRODUCTION

Layer-by-layer (LbL) assembly has recently attracted great attention as a promising method to form defect-free and highly conformal coatings.[1,2] The technique has advantages in chemically controlling the nanoscale local structure, film morphology, and thickness and incorporating a wide range of functional materials. LbL assembly can be driven by either electrostatic or hydrogen bonding. In the first case, the multilayer coating is created by alternatively dipping the substrate into solutions of oppositely charged polyelectrolytes. Assembly by hydrogen bond is applied for compounds of which hydrogen-donor and hydrogen-acceptor groups are available. Control of film growth can be obtained through adjustment of the assembling parameters, such as solution pH for "weak" polyelectrolytes[3,4] or solution ionic strength for "strong" polyelectrolytes,[5,6] and deposition temperature.[7] A wide range of applications utilizing LbL assembly as a fabrication technique has been reported, such as electrochromic devices,[8] solid-state ionic electrolytes,[9,10] proton-exchange membranes for fuel cells,[11] loading/delivery vehicles for biological compounds,[12,13] adhesive layers for cells,[14] humidity sensors,[15] and other nanostructure and microstructure materials.[16,17] Of these applications, electrochromic (EC) devices can benefit most from the LbL assembly, because both electrochromic and electrolyte layers have been successfully formed via this method.[8−10] Currently, high-performance electrochromic devices have been dependent on the use of gel or liquid electrolytes. Although a great number of achievements have been obtained for different types of solid electrolytes, the EC device performance has still been inferior to that with gel or liquid electrolytes.[18,19] The main cause usually has been attributed to the lower ionic conductivity of the solid electrolytes. As a result, achieving good ionic conductivity and better interfacing between solid electrolyte and electrochromic layer is critical to improve device performance.

Polyelectrolytes formed by LbL assembly can be fabricated by both electrostatic and hydrogen bonding. For electrostatic bonding, the choice of polyion pair is deemed important, because it directly affects the number of mobile ions that can be retained, as well as the ionic mobility, which is dependent on the cross-linking density in the assembled films. The combination of water-soluble *linear poly(ethylene imine)* and *poly(acrylic acid)* (LPEI/PAA) has been found to offer some advantages in addressing these problems. The hard Lewis base of the hydrophilic ethylene imine molecules helps to increase the dissolution of alkali metal cations, while the weak polyelectrolyte PAA provides a high amount of mobile counterions under acidic conditions. In the LPEI/PAA system, the pH of the assembling solutions plays an important role in the ionic conductivity, with an increase of one order of magnitude when the pH was increased from 2 to 5. The

Received: December 15, 2010
Revised: March 6, 2011
Published: March 30, 2011

addition of ionic salt after the bilayer film formation increased the conductivity at medium humidity range (52%RH).[9] In the case of hydrogen-bonded *poly(ethylene oxide)/poly(acrylic acid)* (PEO/PAA) system, the addition of ionic salt to the assembly solutions substantially increased the ionic conductivity in the medium humidity range. The reported improvement was up to two orders of magnitude and could tentatively reach above 10^{-4} S/cm for samples measured at 100%RH.[10] Efforts to increase the ionic conductivity with post-assembly treatment, including submersion in a lithium hexafluorophosphate/propylene carbonate solution[20] for PEO/PAA films, in highly acidic solutions,[21] and in oligoethylene glycol (OEG) solution[22] for LPEI/PAA film, showed drastic improvements (up to 9.5×10^{-5} S/cm, as reported in the latter case). It is interesting to note that the treatment of LPEI/PAA film with OEG solution resulted in the increasing plasticization by water and benefited from the intercalation of flexible ethylene glycol molecules into the matrix of the electrostatically bonded bilayer. Reviews of these electrolytes are available in refs 2 and 23 for further reference.

In this report, we explore a new approach using LbL assembly to fabricate a solid polymer electrolyte, which combines electrostatic and hydrogen bonding to obtain high ionic conductivity. The electrolyte consists of four interbonded polymeric layers (and, hence, is termed "tetralayer"). *Linear poly(ethylene imine)* (LPEI) was used in the electrostatic bonding pair with *poly(acrylic acid)* (PAA), while *poly(ethylene oxide)* (PEO) was paired with PAA via hydrogen bonding. LPEI with its heteroatomic hydrophilic backbone has been reported to be favorable for ionic transport in the electrostatically bonded bilayer,[9] while PEO is well-known for its good solubility of lithium salts. The use of PAA is critical, because it serves to bridge the two types of bonding. Characterization of the ionization behavior of PAA has been well-documented,[24] which allows us to derive a suitable combination of assembly parameters, in terms of solution pH and ionic strength. The electrostatically bonded LPEI/PAA could be assembled in the pH range of 2−5, with the best result being obtained at pH 4. Because of the weak interaction, this assembly is unaffected by the presence of ions in the solutions.[9] The assembly of the hydrogen-bonded PEO/PAA was critically dependent on both solution pH and ionic strength. The optimized condition was reported for a pH range of 2−3.5 and salt concentrations of <0.5 M.[10] Although we have attempted deposition with solutions of various pH values (e.g., LPEI/PAA at pH 4 combined with PEO/PAA at pH 2.5) and varied salt concentration (e.g., 0.01−0.5 M), the obtained samples were unstable, in terms of growth and ionic conductivity performance. This was probably due to the mismatched effects of pH and ionic strength to the electrostatic and hydrogen-bond formation. Based on the literature information and our experimental results, we chose a pH value of 3 and an ionic strength of 0.1 M for all of the polyelectrolyte and rinse solutions in the LbL assembly process. Upon establishing the understanding of the tetralayer LbL film in terms of structure, growth, thermal properties, and ionic conductivity performance, we demonstrate the application of this solid electrolyte for electrochromic devices. Designs for transmissive and reflective devices are presented for electrochromic modulation in both the visible and near-infrared (near-IR) wavelength range.

EXPERIMENTAL SECTION

Materials. Polycation LPEI ($M_w \approx 250000$, Polysciences, Inc.) was used as received, as were the polyanion PAA (25 wt % in water, $M_w \approx 200000$, Polysciences, Inc.) and PEO ($M_w \approx 20\,000$ (20K) and 300 000 (300K), Sigma−Aldrich). All of the polyelectrolytes were dissolved in deionized water (Milli-Q system, Millipore Corp.) at a concentration of 0.02 M (with respect to repeating units). Lithium trifluorosulfonate ($LiCF_3SO_3$ or LiTF) (96% pure, Sigma−Aldrich) was dissolved in the polyelectrolytes and rinse solutions at concentration of 0.1 M. The pH was adjusted using dilute perchloric acid ($HClO_4$) (0.1 M) to pH 3 for all the polyelectrolytes and aqueous rinse solutions, unless specified. All the substrates used in the study were cleaned by sonication in series of solutions consisting of acetone, methanol, and deionized water. Right before assembly, the substrates were exposed in a Harrick PCD plasma cleaner for 2 min.

Layer-by-Layer Assembly and Characterization. The layer-by-layer deposition was performed using Carl Zeiss Model HMS70 slide stainer, of which the submerging durations in the polyelectrolyte and rinse baths were preprogrammed to be 15 and 2.5 min, respectively. After deposition was completed, the samples were allowed to dry in ambient (25 °C, ∼52%RH) for at least 3 days before characterization, denoted as "dry state". The "wet state" samples were obtained after exposing the dried ones to an ambient environment of 90%RH in a humidity-controlled chamber at room temperature for 1 h with no liquid being visibly detected on the sample surface.

Tetralayer films were investigated by Fourier transform infrared (FTIR) spectroscopy, using a Perkin−Elmer spectrometer in reflectance mode. The film thickness was measured by surface profilometry using a Tencor-Alpha profilometer. Thick tetralayer films (up to 100 deposition cycles) were deposited on cleaned glass substrates and gently peeled off after drying. These standalone films were employed for studying of their thermal characteristics, using modulated differential scanning calorimetry (MDSC). The samples were first equilibrated at −50 °C, followed by heating to 180 °C, and then cooled back to −50 °C at a fixed rate of 10 °C/min, a period of 60 s, and an amplitude of 1.592 °C. This process was repeated for two measurement cycles. For ionic conductivity characterization, both in-plane and through-plane measurements were performed. For through-plane measurement, films were deposited on a patterned indium-doped tin oxide (ITO) glass substrate, followed by top gold electrode metallization to form cross-bar cells. The in-plane measurement was done using a pair of parallel platinum wires (100 μm in diameter) at a distance of 1 cm. Impedance spectra were obtained using a Solartron Model 1216 system (frequency ≈ 1 MHz−0.1 Hz, $V_{rms} \approx 10-100$ mV) and fitted with Zplot/ZView software. Ionic conductivity measurement, versus temperature, was done in a humidity-controlled chamber with in situ heating via a hot plate.

Electrochromic Device Fabrication. For solid electrochromic device fabrication, LbL electrolyte films were deposited on a transparent ITO−PET substrate (Sigma Aldrich) in transmittance mode. After the samples were dried, a gold grid electrode (0.5 mm in width, with a spacing of 0.5 mm) was formed on top of the LbL film via sputtering. A conducting polymer (polyaniline with dodecylbenzene sulfonic acid (PANI-DBSA)) was used as the active electrochromic layer and drop-cast onto the LBL film that was partially covered by the grid electrode. For reflective devices, the tetralayer electrolyte was first assembled on a

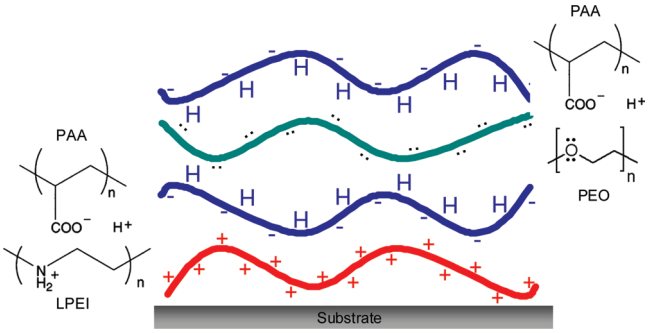

Figure 1. Schematic structure of the tetralayer electrolyte LPEI/PAA/PEO/PAA.

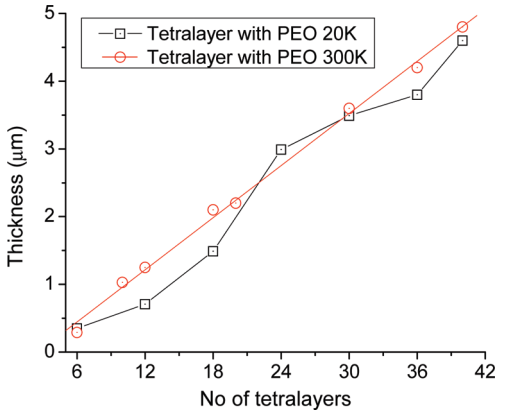

Figure 2. Growth curve for LBL tetralayer films with PEO of molecular weight M_w = 20K and M_w = 300K. Lines are added only as a guide to the eyes.

polycarbonate membrane (pore size of ~10 μm, Whatman), followed by drying in an ambient environment. The gold grid electrode was then deposited on one side of the membrane, as described above. The PANI-DBSA solution was cast on the side with the grid electrode. In the last step, poly(3,4-ethylene dioxythiophene)−poly(4-styrene sulfonic acid) (PEDOT-PSS) was drop-cast on the other side, immediately followed by its attachment to a piece of cleaned aluminum foil, which served as a counter-electrode, and drying in a desiccator for at least 2 h. The electrochromic modulation was measured in the visible to near-IR range (300−2000 nm), using a Perkin−Elmer UV−vis−NIR spectrometer, and applying constant bias accordingly, using an Autolab potentiostat.

RESULTS AND DISCUSSION

Film Growth and Thickness Profile. Figure 1 shows the schematic structure of the tetralayer electrolyte LPEI/PAA/PEO/PAA. The proposed structure started with the LPEI and first PAA layers that were attached to each other via electrostatic bonding between the amine and ionized carboxylic groups. Because of the partial ionization and protonation of this PAA layer, it allowed the protonated carboxylic acid groups COOH to contribute to the hydrogen bonding with the ether oxygen in the next PEO layer. This PEO layer again participated in the hydrogen bonding with the second PAA layer, of which the partial ionization of COO^- groups enabled the electrostatic bond with the subsequent LPEI layer to start a new assembly cycle.

The growth behavior of the dried tetralayer films is shown in Figure 2. While films with PEO300K grew linearly throughout the examined thickness range, films with PEO20K showed nonlinear growth up to 24 tetralayers, followed by a more-linear manner. The thickness of each tetralayer for linear growth was 115 ± 8 nm and 112 ± 7 nm for tetralayers with PEO20K and PEO300K, respectively, which was slightly lower than the thickness of the PAA/PEO bilayer (as mentioned above). On the other hand, if one considered the reported thickness for the single bilayer LPEI/PAA (25 nm, pH 3)[9,25]) and PEO/PAA (80 nm, pH 3, 0.1 M $LiCF_3SO_3$)[20] in films with 20 or more deposition cycles, it could be seen that the tetralayer thickness here was in the same range as the total thickness of both of these bilayers combined. Note that the appearance of ions from LiTF salt during the tetralayer assembly could affect the deposition of the LPEI/PAA portion in which the polyions assumed "a loopier and less-extended surface conformation" due to screening-enhanced adsorption.[10,26] This conformation subsequently abated the number of the protonated COOH groups on the assembled PAA layers that were available for hydrogen bonding with the PEO molecules. Overall, it could be expected that the LPEI/PAA portion was slightly thicker, while the PEO/PAA portion was thinner in the tetralayer, compared to each of the bilayers alone. The bonding between Li^+ cations and PAA and PEO molecules, shown in the FTIR characterization, could also reduce both electrostatic and hydrogen bonding in the tetralayer film formation. Therefore, the growth profile suggested that these behaviors exerted a more obvious impact during the early stage of the tetralayer films, with PEO20K showing a superlinear characteristic. On the other hand, films with PEO300K only exhibited linear growth, with only subtle influence by the chain conformation.

FTIR Analysis. To understand the combined formation of electrostatic and hydrogen bonding in the tetralayer electrolyte, we have examined the characteristics of each single bond in bilayer structure, namely, LPEI/PAA and PEO/PAA. The infrared spectroscopic data showed clear differences in the bonding characteristics of the two bilayer structures. For the PEO/PAA bilayer, the absence of the ionized carboxylic group COO^- at 1554 cm^{-1} and strong interaction signal of the carboxylic acid−ether oxygen at 1732 cm^{-1} indicated the successful formation of hydrogen bonding. Besides, free $CF_3SO_3^-$ ions were also detected by the symmetric stretching of SO_3^- group at 1032 cm^{-1}. On the other hand, strong COO^- (1558 cm^{-1}) and weak amine (1606 cm^{-1}) bands were observed for the LPEI/PAA bilayer even at pH 3. This confirmed the existence of electrostatic bonding, despite the low level of ionization of PAA molecules at low pH values. More information of these results is available in the Supporting Information (see Figure S1). The existence of the electrostatic and hydrogen bonding in LbL-assembled bilayer films under unified conditions of pH 3 and a salt concentration of 0.1 M in solution enabled the combination of both of these bonds into a single structure via the LbL method.

Infrared spectra for tetralayer samples in dry and wet state are presented in Figure 3. The hydroxyl stretching region (3800−2200 cm^{-1}, Supporting Information, Figure S2) of the dry-state samples indicated a mixture of various modes such as noncyclic single or multiple hydrogen bonds, cyclic dimers, and free hydroxyl groups, which is similar to a previous report.[27] For the wet-state samples, the hydroxyl bands showed the dominant existence of noncyclic single or multiple hydrogen bonds and cyclic dimers, compared to the free hydroxyl groups. This was

dx.doi.org/10.1021/cm103572q |Chem. Mater. 2011, 23, 2142–2149

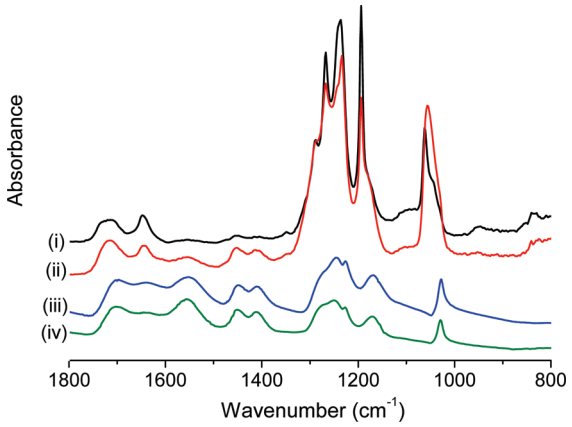

Figure 3. FTIR data for tetralayer LBL films with PEO a molecular weight of 20K (spectra i, iii) and 300K (spectra ii, iv) in the wet state (spectra i, ii) and the dry state (spectra iii, iv).

caused by the higher moisture content in the samples, which is due to the exposure humidity (90%RH for 2 h); this led to more flexibility in the polymer chains and weakening of the intermolecular hydrogen bond.

In the 1800−800 cm^{-1} region, significant changes in the carbonyl stretching (1750−1700 cm^{-1}) and the PEO-LiTF complex (1100−800 cm^{-1}) could be seen for the dry-state and wet-state samples. For the former, possible convolution of the carboxylic-ether oxygen (1732 cm^{-1}) and carboxylic dimer (1699 cm^{-1}), as discussed earlier for the PAA/PEO bilayer, resulted in the broad composite bands centered above 1700 cm^{-1}. For the dry-state samples, the carbonyl bands were broader and centered toward lower wave numbers (~1700 cm^{-1}). The broad COO^- bands (~1556 cm^{-1}) similarly observed in the two LPEI/PAA bilayer samples also became more visible in the dried tetralayer samples. The existence of intermolecular hydrogen bonding and the lower carbonyl absorption bands could be explained by neutralization of the COO^- groups and formation of the Li^+-COO^- compound. It has been reported that the phase separation in the PAA/PEO blend occurs with the increased neutralization of the acrylic acid groups. This is reflected by the shift to lower wave numbers for the carbonyl band and to higher wave numbers for the COO^- band, signifying the larger fraction of the acid dimers and the stronger Li^+-COO^- dipoles in the microphase-separated aggregates.[27] For the dry-state samples in our study, the COO^- bands were unchanged at ~1556 cm^{-1} as compared to ~1554 cm^{-1} of the wet-state. Hence, it is believed that phase separation between PEO and LPEI/PAA could have taken place in the dry tetralayer, because of the formation of more carboxylic dimers, and the Li^+ ions were only loosely bound by the COO^- groups, forming complex compounds with the separated PEO chains.

The three sharp bands at 1267, 1236, and 1193 cm^{-1} arose from the superimposing of signals contributed from both LPEI and PEO molecules in the region of 1340−1130 cm^{-1}. The strong bands at 1057 (tetralayer 300K) and 1063 (with a shoulder band at 1043) cm^{-1} (tetralayer 20K) corresponded to a mixture of COC stretching and CH_2 rocking, which is close to the bands observed for pure PEO.[28,29] These vibrational signals, which were also characterized by the 950 and 840 cm^{-1} bands, appeared in the wet-state sample but not in the dry-state samples. This corroborated the above observation of the phase separation of PEO, which is due to the decrease in intermolecular hydrogen bonding and the formation of Li-ether oxygen compounds. For the dry-state samples, bands at 1029 cm^{-1} were attributed to the SO_3 symmetric stretching that corresponds to the "free" state of the triflate ions.[30,31] The disappearance of the vibrational bands of COC stretching and CH_2 rocking at 950 and 840 cm^{-1}, which is characteristic to a pure PEO backbone, further underlined the dissolution of the ionic salt into the tetralayer structure, even in the dry state.

However, note that the structure of polymer assembly and the binding of Li^+ ions might not be the only mechanisms that governed the ionic transport. The medium through which these Li^+ ions are transported also could have a major impact. Therefore, the difference between the wet and dry states observed here might not be only due to the solubility differences of lithium, but also due to the interaction between lithium cations and the water content or the polymer matrix. To examine this hypothesis, the dry-state samples were heated to 180 °C for 15 min and the IR spectroscopic data were collected once the samples were cooled to room temperature (data are available in the Supporting Information (see Figure S3)). Clear evidence of amide formation via thermal cross-linking between the amine and carboxylic groups (LPEI and PAA) appeared for both of the tetralayer samples (with PEO20K and PEO300K). Furthermore, a stronger signal of CH_2 twisting mode from PEO could be observed, which was possibly indicative of structural change of this polymer. It will be shown in the subsequent sections that these changes were related to the reduced ionic conductivity of the tetralayer electrolyte, which was due to changes in structural formation.

Thermal Analysis. The thermal properties of the LBL tetralayer films, characterized by modulated DSC, are shown in Figure 4 for two measurement cycles. During the first heating cycle, broad endothermic peaks that had nonreversing characteristics dominated the thermal process. The peak temperatures were 94 °C and 107 °C for tetralayer films with PEO20K and PEO300K, respectively, while heat-enthalpy values were 279.6 ± 0.2 J/g for both samples determined from the nonreversing curves (see Figure 4a). Similar strong and broad peaks existing only in the first heating cycle have been observed in the *poly(sodium 4-styrene sulfonate) /poly(diallyldimethylammonium chloride)* (PSS/PDAC) blended polyelectrolyte system and attributed to the evaporation of water residue after freeze-drying.[32] On the other hand, thermal study of a PEO/LiTF blend also showed a broad transition in the range of 70−180 °C, which was due to the melting of the Li−O complex (with a cation:oxygen ratio of ~1:20).[29] Since both of the samples were fabricated using identical processes, the similar enthalpy values here possibly suggest the dominance of moisture evaporation from the samples. Despite not being observed by the DSC results, the thermal cross-linking process should also be included in the broad nonreversing curves. The existence of the very broad transition in the range of 60−100 °C on the reversing curves during the first heating cycle indicated the presence of the unbound PEO molecules that formed microcrystalline sites and a complex compound with the Li^+ cations. The existence of the polymer-salt compounds was previously confirmed by the detection of the "free" triflate ions in both samples, as described by the FTIR data above.

Glass-transition temperatures of 2 °C (tetralayer PEO20K) and 9 °C (tetralayer PEO300K) were observed from the reversing curves for both samples (see Figure 4a1). The reported glass-transition temperature of a PEO/PAA bilayer with LiTF was ~50 °C, compared to ~30 °C for the neat bilayer.[18] Both of

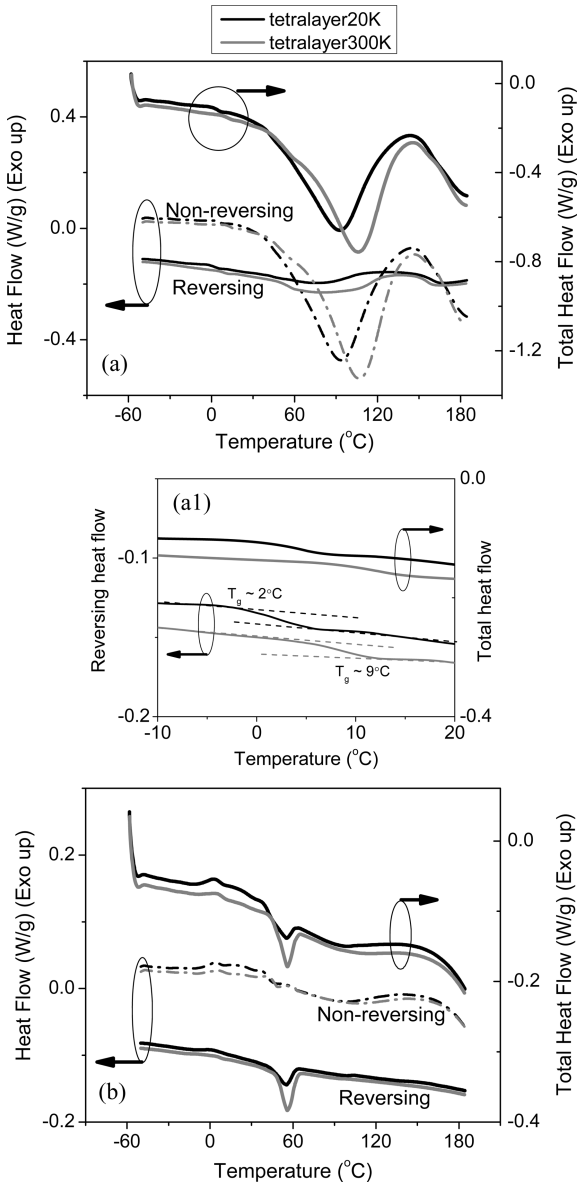

Figure 4. Modulated DSC data for tetralayer of PEO20K and PEO300K during (a) the first heating cycle (with panel a1 showing the enlarged region of the reversing and total heat flow curve (from −10 °C to 20 °C), and (b) second heating cycle.

these values resided between the glass-transition temperatures of PEO ($T_g \approx -56$ °C) and PAA ($T_g \approx 99$ °C), and their difference was suggested to be indicative of the reduction of PEO content in the presence of ionic strength.[33] On the other hand, determination of the glass transition for the LPEI/PAA bilayer alone has been reported to be rather difficult, because LPEI is a highly crystalline polymer. Since the bilayer existed as a polyionic complex homogeneous blend, the glass-transition behavior of the LPEI/PAA matrix was considered to be governed by the upper bound of the PAA glass-transition temperature for films with a low absorbed moisture content.[33] The detection of much-lower T_g values for the dried tetralayer films in our study indicated a homogeneous assembly of hydrogen-bonded PEO/PAA and electrostatically bonded LPEI/PAA in the film matrix, with possibly more-dominant effect of the former.

Figure 4b presents the second heating cycles of the same tetralayer samples. The thermal analysis data were dominated by a single sharp endothermic peak at ~55−56 °C for both tetralayer films. These values were exactly the same as the melting temperature of PEO from the blend with LiTF, which was measured separately. The melting enthalpy for tetralayer with PEO300K is 6.81 J/g, almost doubling the value for tetralayer with PEO20K, ~3.85 J/g. Small exothermic features were also seen before the melting peaks in both curves, which were fully reflected in the nonreversing curve; this is attributed to cold crystallization and crystal perfection of the PEO phase and the complex compounds. From the analysis of the growth curves, the tetralayer PEO300K samples should consist of a more-regulated and more-homogeneous assembly of the molecular layers, based on the observed linear profile. Therefore, more bonding formation of the electrostatic (between imine and ionized carboxylic groups) and hydrogen (between ether oxygens and protonated carboxylic groups on the same PAA molecules) type could be expected in this sample. The larger melting enthalpy obtained in the second heating cycle for tetralayers with the PEO300K sample indicated that more PEO crystalline phase was formed, because of the longer polymer chains. As a result, this possibly signified the breaking of bonds between the hydrogen donor−acceptor layers, especially PEO/PAA, during the first heating cycle and followed by the rearranging of polymer chains during the cooling phase. For the tetralayer with the PEO20K sample, the "loopier and less-extended surface conformation" of the deposited polyionic layers in the early growing stage possibly reduced the extent of bonding formation. This allowed the PEO chains to be confined to groups of unbound molecules, which formed small-size crystallites after the first heating cycle. The obtained thermal results suggested that the crystalline PEO phase should exist in a lower equilibrium energy state and is more thermodynamically favorable than the bonded state between PEO and PAA molecules. The activation energy for the association of PAA and PEO molecules in aqueous media has been reported to be 3.7 kcal/mol, while the value for dissociation was 2.8 kcal/mol. The entropy value for dissociation was also found to be more negative, compared to that of association.[34] Hence, it could be suggested that the hydrogen bonding between PAA and PEO was not fully stable and could be broken during the heating cycle.

Electrical Characterization. To elucidate the application of the tetralayer films as solid polymer electrolytes, electrical characterizations were performed, as shown in Figure 5. Ionic conductivity values were extracted from both wet-state and dry-state samples, as summarized in Table 1. Tetralayers with PEO20K films showed slightly higher conductivity values, compared to those with PEO300K in the similar state. Overall, the similar ionic conductivity for both in-plane and through-plane measurement in each sample indicated isotropic conducting characteristics and good intermixing of the participating polymer, rather than stratified layer formation. The increment of one order of magnitude when the samples were exposed to high relative humidity (90%RH) indicated the critical effect of water plasticization in the LBL-assembled film to the ionic conduction. Detailed characterizations of ionic conductivity behavior for LPEI/PAA and PAA/PEO bilayers have showed similar dependence of conductivity values on the relative humidity.[9,10,20,21] The higher values for the samples with PEO20K in both states further supported the structural difference of the tetralayer films, as discussed above. Since the hydrogen bonding between

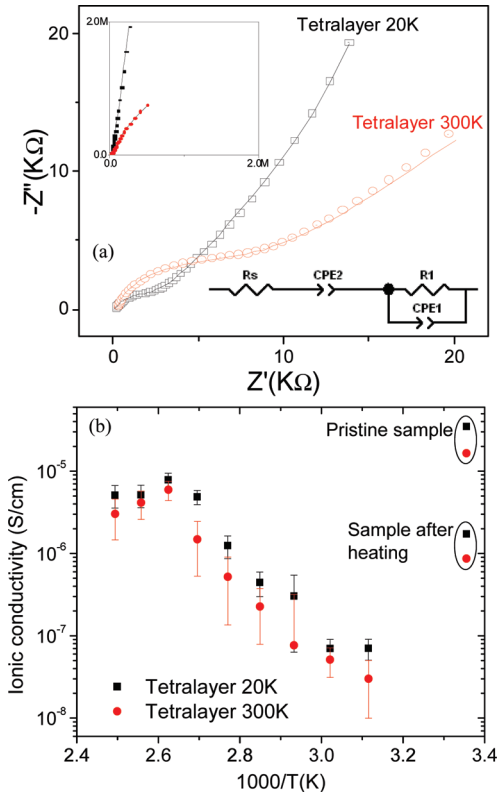

Figure 5. Electrical characterization performed on the tetralayer solid electrolyte: (a) Nyquist plot of tetralayer films with fitting shown by the lines (the insets show the full-scale data and the fitting circuit), and (b) ionic conductivity measured against temperature.

Table 1. Ionic Conductivity of Tetralayer LBL Films in Wet and Dry State

sample	wet state (90% RH)	dry state (52%RH)
Tetralayer with PEO20K		
in-plane	9.1×10^{-4} S/cm	5.3×10^{-5} S/cm
through-plane	8.5×10^{-4} S/cm	4.8×10^{-5} S/cm
Tetralayer with PEO300K		
in-plane	6.8×10^{-4} S/cm	1.7×10^{-5} S/cm
through-plane	1.7×10^{-4} S/cm	1.3×10^{-5} S/cm

PEO300K and PAA was more homogeneous, the amount of ether oxygen available to dissolve LiTF salt was reduced. This led to less-dissociated mobile ions in the tetralayer matrix. In contrast, because of the assembly of loopier polymer layers, the shorter PEO molecules had a tendency to accumulate at locations that were rich in unbound ether oxygen, which helped to enhance the dissolution of the ionic salt.

Ionic conductivity data of the tetralayer samples measured against temperature are shown in Figure 5b. The decrease in ionic conductivity from room temperature (denoted as "pristine sample" in Figure 5b) to 50 °C was caused by the removal of moisture traces in the sample. In situ measurement by hygrometer showed less than 10%RH existed in the test ambient from 50 °C onward. Therefore, the increment of conductivity values at higher temperatures was deemed independent of the moisture content in the LBL sample. The conductivity in both samples increased as the temperature increased up to 110 °C, then exhibited a slight reduction. Similar conductivity behavior has been reported for the electrostatically bonded PSS/PDAC system, which was mainly attributed to the loss of moisture trace in the prepared samples. Data obtained from the second measurement of these same samples showed a three-order-of-magnitude reduction in the conductivity for the entire temperature range of testing.[32] Another explanation for the decrease in conductivity values has been linked to the thermal cross-linking between the amine and carboxylic groups to form amide products in the *poly(allylamine hydrochloride)/poly(acrylic acid)* (PAH/PAA) system. This process resulted in more-rigid bonding and repressed motion of polymer chains, leading to an increment in the film resistance of three orders of magnitude.[35] In our experiment, the conductivity at room temperature obtained in the second measurement only exhibited a one-order-of-magnitude reduction, while the high-temperature data closely followed the data obtained in the first measurement. This indicates that the thermal cross-linking in the tetralayer LbL samples was of lesser extent, compared to the reported PAH/PAA bilayer. Based on the characteristics of conductivity data observed here, some conclusions can be drawn. First, the increment of conductivity in the early stage of heating was mainly facilitated by the softening of the polymer chains and was independent of the moisture in the samples. Thermal cross-linking between LPEI and PAA possibly occurred, starting from 100 °C, but was limited by the breaking of PEO/PAA bond and the crystallization of PEO. Lastly, the ionic conductivity of the heat-treated samples was limited by the rigid cross-linked network of polymer chains in the subsequent measurement.

Table 2. Fitting Parameters for the Vogel−Fulcher−Tammann (VFT) Equation

	σ_0 (S/cm)	B	T_0 (K)
tetralayer with PEO20K	1.1×10^{-8}	648.78	224
tetralayer with PEO300K	1.7×10^{-8}	280.39	433

The Vogel−Fulcher−Tammann (VFT) equation was used to fit the conductivity data shown in Figure 5b, following the method reported in ref 36. In the VFT equation shown below, σ_0 is the pre-exponential factor or the conductivity at infinitely high temperature, B has the dimension of energy and is related to the activation of ionic conduction, and T_0 is the temperature at which σ approaches a value of zero. The fitting parameters are presented in Table 2.

$$\sigma = \sigma_0 \exp\left(-\frac{B}{T - T_0}\right)$$

The intrinsic conductivity (σ_0) values were found to be similar for both samples, which possibly underlined the effect of LPEI/PAA ionic cross-linking to charge transport in the tetralayer polyelectrolyte. On the other hand, the T_0 values reflected the difference in the structure of the tetralayer samples. For the tetralayer with PEO20K, $T_0 \approx -49$ °C is close to the PEO glass-transition temperature, whereas a value of $T_0 \approx 160$ °C for tetralayers with PEO300K indicates more influence by PAA and possibly greater interaction of both electrostatic and hydrogen bonding between the polyionic layers, as discussed above.

Electrochromic Device Fabrication and Characterization. Figure 6 presents two different device designs for the application of the LbL electrolyte film for electrochromics. For both types of devices, as negative bias was applied to the working (gold grid)

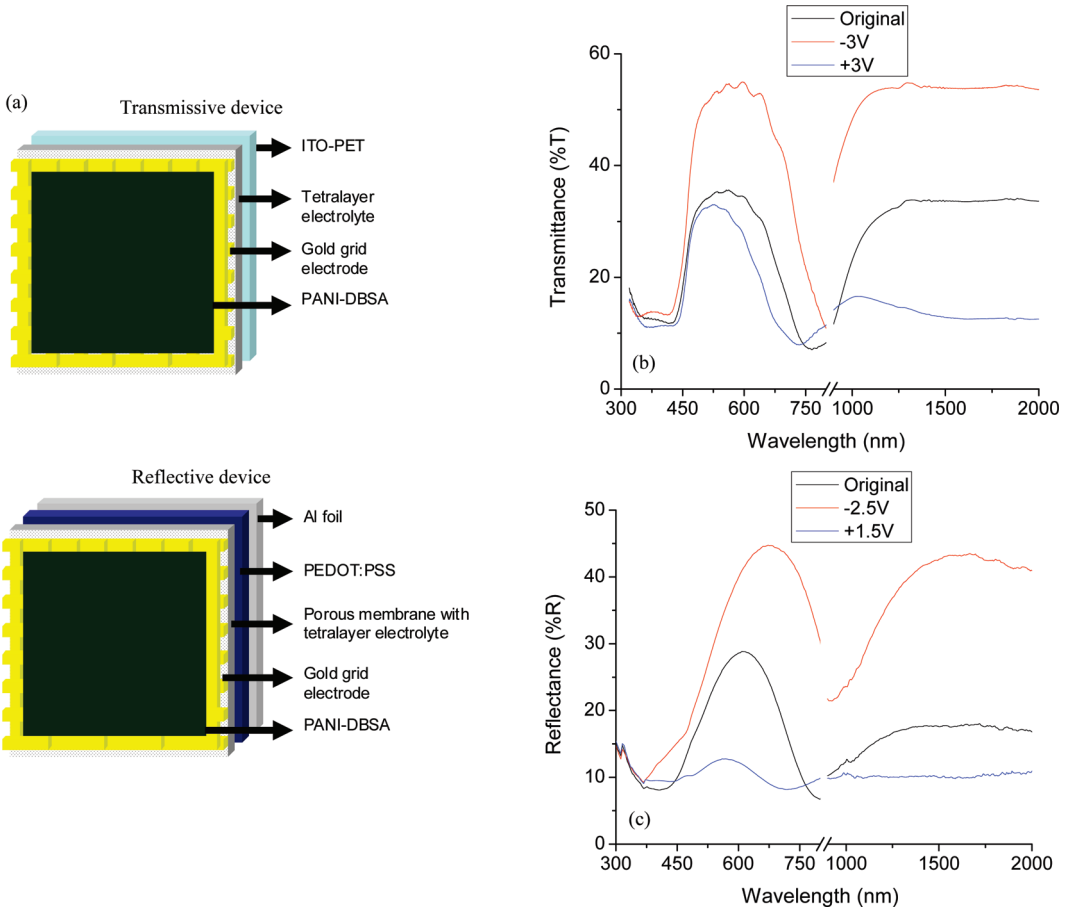

Figure 6. (a) Schematic of the electrochromic device structures. (b) Performance of a transmissive device with a tetralayer polyelectrolyte comprised of PEO20K. (c) Performance of a reflective device with a tetralayer polyelectrolyte comprised of PEO20K.

electrode, the electrochromic PANI-DBSA layer was oxidized and became transparent to the incoming light. This allowed the light beam to pass through the transparent ITO-PET substrate in the transmission mode, while the light beam was reflected by the grid electrode in the reflection mode (see Figure 6a). In the reversed reaction upon applying positive bias, the PANI-DBSA layer became absorptive to the incoming light. The electrochromic behavior was driven by the transport of mobile ions between the PANI-DBSA and the solid LBL electrolyte. The highest obtained modulation is ~38% at a wavelength of 670 nm for the transmissive and reflective devices. The values are slightly smaller (~35%) in the near-IR region (1100−2000 nm), as shown in Figures 6b and 6c. The reported modulation values for transmissive devices comprised of transparent electrodes and semisolid polymer electrolyte were in the range of 25%−50%.[18] A similar device structure, using a porous membrane but with an uninterrupted electrode, has been reported to yield up to 40% modulation in the near-IR range.[18,19] Based on these available reported data, it is believed that the solid electrochromic devices using LbL-assembled electrolytes can achieve comparable performance with room for further improvement. Optimization of the interface between the electrolyte and the electrochromic layer is one of the possible strategies. The use of LbL assembly indeed has a great advantage in obtaining this. The method can provide a continuous formation of the electrolyte and the electrochromic device, which can enhance the ion exchange during the electrochromic modulating process.

CONCLUSION

We have examined a new type of polyelectrolyte that combines electrostatic and hydrogen bonding into multilayer structure formed via layer-by-layer (LbL) assembly. The polyelectrolytes showed improvements in ionic conductivity, because of the hydrophilic linear poly(ethylene imine) (LPEI) backbones, which allow better ionic transport, because of the flexible chains and the enhancement of Li^+-ion dissolubility by incorporating poly(ethylene oxide) (PEO). The molecular weight of PEO had a direct effect on the structure of the tetralayer, with the longer molecules having more homogeneous hydrogen bonding to the electrostatic linear poly(ethylene imine)/poly(acrylic acid) (LPEI/PAA) layer. Shorter PEO molecules had limited hydrogen bonding and loopier formation, which provide more ether oxygen locations for the dissolution of Li salt. Thermal study of the tetralayer samples showed ionic transport through segmental motions governed by the Vogel−Fulcher−Tammann (VFT) equation. Thermal cross-linking to form amide product and breaking of the hydrogen bond that leads to separated crystalline PEO phase were observed. However, because of the competition between these two processes, the ionic conductivity did not suffer critical depression, as observed in the reported bilayer structure. Designs for electrochromic devices using the tetralayer electrolyte were demonstrated for both the transmissive and reflective modes. The performance in the visible and near-infrared range was comparative to devices that use polymer

electrolytes in the semisolid state. This, hence, enables the realization of complete solid-state electrochromic devices using polymeric materials.

■ ASSOCIATED CONTENT

Supporting Information. FTIR data for various sample of LbL-assembled bilayer and tetralayer structures. This material is available free of charge via the Internet at http://pubs.acs.org.

■ AUTHOR INFORMATION

Corresponding Author

*E-mail addresses: pslee@ntu.edu.sg (P.S.L.), hammond@mit.edu (P.T.H.).

Present Addresses

[||]Brady Corporation Asia Pte, Ltd., 1 Kaki Bukit Crescent, Singapore 416236.

■ ACKNOWLEDGMENT

The authors would like to acknowledge the financial support from DSTA and Temasek Laboratories @NTU (Project No. POD0713908).

■ REFERENCES

(1) Decher, G. *Science* **1997**, *277*, 1232.
(2) Hammond, P. T. *Adv. Mater.* **2004**, *16*, 1271.
(3) Yoo, D.; Shiratori, S. S.; Rubner, M. F. *Macromolecules* **1998**, *31*, 4309.
(4) Shiratori, S. S.; Rubner, M. F. *Macromolecules* **2000**, *33*, 4213.
(5) Lvov, Y.; Decher, G.; Mohwald, H. *Langmuir* **1993**, *9*, 481.
(6) Clark, S. L.; Montague, M. F.; Hammond, P. T. *Macromolecules* **1997**, *30*, 7237.
(7) Quinn, J. F.; Caruso, F. *Macromolecules* **2004**, *20*, 20.
(8) DeLongchamp, D. M.; Kastantin, M.; Hammond, P. T. *Chem. Mater.* **2003**, *15*, 1575.
(9) DeLongchamp, D. M.; Hammond, P. T. *Chem. Mater.* **2003**, *15*, 1165.
(10) DeLongchamp, D. M.; Hammond, P. T. *Langmuir* **2004**, *20*, 5403.
(11) Argun, A.; Ashcraft, J. N.; Hammond, P. T. *Adv. Mater.* **2008**, *20*, 1539.
(12) Kozlovskaya, V.; Sukhishvili, S. A. *Macromolecules* **2006**, *39*, 5569.
(13) Kharlampieva, E.; Sukhishvili, S. A. *Langmuir* **2004**, *20*, 9677.
(14) Yang, S. Y.; Mendelsohn, J. D.; Rubner, M. F. *Biomacromolecules* **2003**, *4*, 987.
(15) Yang, S.; Zhang, Y.; Guan, Y.; Tan, S.; Xu, J.; Cheng, S.; Zhang, X. *Soft Matter* **2006**, *2*, 699.
(16) Li, Q.; Quinn, J. F.; Caruso, F. *Adv. Mater.* **2005**, *17*, 2058.
(17) Yang, S. Y.; Kim, D. Y.; Jeong, S. M.; Park, J. W. *Macromol. Rapid Commun.* **2008**, *29*, 729.
(18) Nguyen, C. A.; Xiong, S.; Ma, J.; Lu, S.; Lee, P. S. *J. Phys. Chem. B* **2009**, *113*, 8006.
(19) Chandrasekhar, P.; Zay, B. J.; Birur, G. C.; Rawal, S.; Pierson, E. A.; Kauder, L.; Swanson, T. *Adv. Funct. Mater.* **2002**, *12*, 95.
(20) Lutkenhaus, J. L.; McEnnis, K.; Hammond, P. T. *Macromolecules* **2007**, *40*, 8367.
(21) Lutkenhaus, J. L.; McEnnis, K.; Hammond, P. T. *Macromolecules* **2008**, *41*, 6047.
(22) Lowman, G. M.; Tokuhisa, H.; Lutkenhaus, J. L.; Hammond, P. T. *Langmuir* **2004**, *20*, 9791.
(23) Kharlampieva, E.; Kozlovskaya, V.; Sukhishvili, S. A. *Adv. Mater.* **2009**, *21*, 3053.
(24) Choi, J.; Rubner, M. F. *Macromolecules* **2005**, *38*, 116.
(25) Zacharia, N. S.; DeLongchamp, D. M.; Modestino, M.; Hammond, P. T. *Macromolecules* **2007**, *40*, 1598.
(26) Stuart, M. A. C.; Tamai, H. *Langmuir* **1988**, *4*, 1184.
(27) Lu, X.; Weiss, R. A. *Macromolecules* **1995**, *28*, 3022.
(28) Lee, J. Y.; Painter, P. C.; Coleman, M. M. *Macromolecules* **1988**, *21*, 346.
(29) Frech, R.; Chintapalli, S.; Bruce, P. G.; Vincent, C. A. *Macromolecules* **1999**, *32*, 808.
(30) Schantz, S.; Sandahl, J.; Borjesson, L.; Torell, L. M.; Stevens, J. R. *Solid State Ionics* **1988**, *28−30*, 1047.
(31) Schantz, S.; Torell, L. M.; Stevens, J. R. *J. Appl. Phys.* **1988**, *64*, 2038.
(32) Imre, W.; Schonhoff, M.; Cramer, C. *J. Chem. Phys.* **2008**, *128*, 134905.
(33) Yoo, P. J.; Nam, K. T.; Belcher, A. M.; Hammond, P. T. *Nano Lett.* **2008**, *8*, 1081.
(34) Bednar, B.; Morawetz, H.; Shafer, J. A. *Macromolecules* **1984**, *17*, 1634.
(35) Harris, J. J.; DeRose, P. M.; Bruening, M. L. *J. Am. Chem. Soc.* **1999**, *121*, 1978.
(36) Stickel, F.; Fischer, E. W.; Richert, R. *J. Chem. Phys.* **1995**, *102*, 6251.